Ergodic Capacity of a Vertical Underwater Wireless Optical Communication Link Subject to Misalignment

Ikenna Chinazaekpere Ijeh, Oussama Haddad, Mohammad Ali Khalighi

Ergodic Capacity of a Vertical Underwater Wireless Optical Communication Link Subject to Misalignment

1st Ikenna Chinazaekpere Ijeh
Department of Electrical/Electronic Engineering
Alex Ekwueme Federal University Ndufu-Alike Ikwo
Ebonyi State, Nigeria
Ikenna.Ijeh@funai.edu.ng

2nd Oussama Haddad
Aix Marseille University, CNRS
Centrale Marseille, Institut Fresnel
Marseille, France
Oussama.Haddad@fresnel.fr

3rd Mohammad Ali Khalighi
Aix Marseille University, CNRS
Centrale Marseille, Institut Fresnel
Marseille, France
Ali.Khalighi@fresnel.fr

***Abstract*—Typical underwater communication scenarios include data transfer between a surface platform and an underwater unit. We consider the use of underwater wireless optical communications (UWOC) for such scenarios, where the link performance is affected by transmitter-receiver misalignment in practice. The focus is on the channel ergodic capacity based on an elaborate statistical model of the aquatic channel accounting for different phenomena such as surface wind speed, beam directivity, underwater unit beam misalignment, and solar noise, as well as the transmitter/receiver parameters. The presented results demonstrate the channel effects and provide interesting insight into the design of such links.**

***Index Terms*—Underwater wireless optical communications; Link misalignment; Ergodic capacity; Silicon photo-multiplier.**

I. Introduction

Underwater wireless optical communication (UWOC) systems are rapidly becoming major players in the application domains requiring high-speed data transmission over short-to-moderate ranges. Their advantage over the traditional acoustic communications include lower implementation cost, lower energy consumption, as well as much smaller latency and higher data rates [1]. These optical links, however, are subject to water absorption and scattering, transmitter (Tx) - receiver (Rx) link misalignment, solar noise, and oceanic turbulence [2]. These factors adversely affect the signal captured at the Rx, degrading and limiting hence the system performance.

A typical application scenario is the data transfer between an underwater unit, such as an autonomous underwater vehicle (AUV), and a surface platform, such as a buoy. The performance of such a vertical link is, in particular, susceptible to link misalignment due to sea surface roughness initiated by wind, ocean currents, etc., and instability of the underwater unit, hence affecting the link capacity. Several research works have studied the impact of misalignment in UWOC vertical links. Considering the impact of random sea surfaces, [3] studied for both upload and download cases the interest of system parameter optimization. Also, [4] and [5] investigated a buoy-based UWOC downlink scenario, of which the latter extended in [6] to the case of employing multiple Txs and Rxs to improve channel capacity. An angular multiple-input multiple-output technique was proposed in [7], to reduce misalignment effect for the case of UWOC links over relatively short ranges. Meanwhile, non-line-of-sight data transmission between underwater units (using reflection from the sea surface) was studied in [8], [9].

In this paper, we consider the downlink scenario between a buoy and an AUV beneath it, as illustrated in Fig. 1. The link could be for control data download from a sea surface observation station to the AUV. A light-emitting diode (LED) is considered at the Tx and a high sensitivity silicon photo-multiplier (SiPM) at the Rx, with the intent to improve the maximum achievable link range [10]. We study the ergodic capacity performance of this vertical UWOC link, and demonstrate, through numerical results, the effects of link and Tx-Rx parameters on the system performance. To the best of our knowledge, this study is the first in its kind that takes into account the effects of link misalignment and solar radiations.

The remainder of this paper is organized as follows. Section II introduces the channel and system model of the considered UWOC link. The performance metric, i.e., the ergodic capacity and its calculation are described in Section III. Then, numerical results are presented in Section IV to investigate the effects of channel conditions and system parameters on the ergodic capacity. Lastly, Section V concludes the paper.

II. Channel and System Model

We consider an intensity modulation and direct detection (IM/DD) scheme using an uncoded non-return to zero (NRZ) on-off keying (OOK) signal modulation. After propagating through the aquatic medium, the optical power P_{Rx} of the received signal, captured on the Rx lens, is related to the transmitted power P_{Tx} and the channel coefficient h as:

$$P_{\text{Rx}} = P_{\text{Tx}}\, h, \tag{1}$$

This work was partly supported by Alex Ekwueme Federal University Ndufu-Alike (AE-FUNAI) in partnership with the Embassy of France in Nigeria and Campus France. It was also based upon work from European Union's Horizon 2020 COST Action CA19111 NEWFOCUS (European network on future generation optical wireless communication technologies).

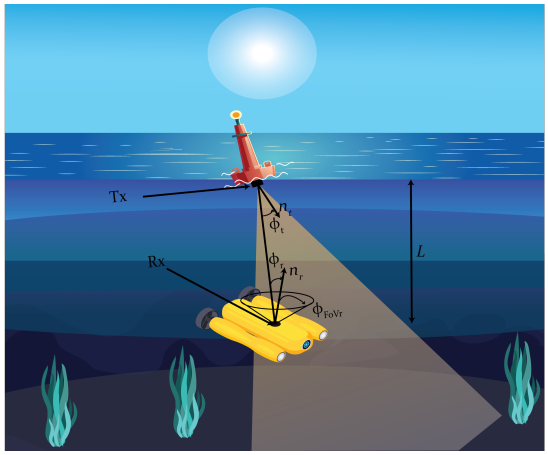

Fig. 1. Illustration of the considered UWOC downlink from buoy to AUV.

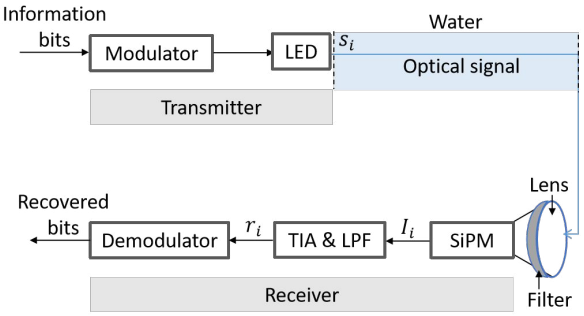

Fig. 2. The block diagram of the UWOC communication link.

$$h = \underbrace{\frac{m+1}{2\pi}\frac{A_{\text{PD}}\,T_{\text{s}}\,g}{L^2}\,e^{-(L\,K_{\text{d}})}}_{h_c}\underbrace{\cos^m(\phi_{\text{t}})}_{h_{\phi_{\text{t}}}}\underbrace{\cos(\phi_{\text{r}})}_{h_{\phi_{\text{r}}}}\underbrace{\Pi\Big(\frac{\phi_{\text{r}}}{\phi_{\text{FoVr}}}\Big)}_{h_a}, \tag{2}$$

where m denotes the Lambertian order of the Tx radiation pattern, A_{PD} is the active area of the photo-detector (PD), T_{s} is the signal transmission of the optical filter and $g = \frac{{n_{rf}}^2}{\sin^2(\phi_{\text{FoVr}})}$ is the gain of a non-imaging concentrator lens with refractive index n_{rf} and Rx field of view (FoV) ϕ_{FoVr}. Also, L is the link distance, K_{d} denotes the diffuse attenuation coefficient [11] while $\phi_{\text{t}} \in \{0, \frac{\pi}{2}\}$ and $\phi_{\text{r}} \in \{0, \frac{\pi}{2}\}$ are the angle of irradiance at the Tx and the incidence angle at the Rx respectively [12]. Lastly, $\Pi(u) = 1$ if $u \leq 1$, and zero otherwise.

The captured signal intensity at the Rx lens generates a photo-current I_i at the SiPM output (see Fig. 2), which is expressed as:

$$I_i = \underbrace{\mathcal{R}_{\text{e}}\,s_i\,h}_{I_{s,i}} + I_d + I_b + n_{s_i} = \breve{I}_i + n_{s_i}, \tag{3}$$

where $\mathcal{R}_{\text{e}}$ is the SiPM responsivity [13], $I_{s,i}$ represents the useful OOK signal s_i, $i \in \{0, 1\}$, associated to transmitted optical powers P_{Tx_0} and P_{Tx_1} for bits '0' and '1' respectively, and related to an extinction ratio, $\alpha = P_{\text{Tx}_0}/P_{\text{Tx}_1}$. Also, I_d is the dark current, I_b is due to the background radiations, and n_{s_i} is the Rx noise, including shot noise, dark current noise, and background noise. We have [14]:

$$I_b = \mathcal{R}_{\text{e}}\,E_{\text{sun}}(\lambda, L)\,\pi\phi^2_{\text{FoVr}}\,T_w\,T_f\,B_o\,A_{\text{PD}}, \tag{4}$$

where $E_{\text{sun}}(\lambda, L) = E_{\text{sun}}(\lambda, 0)\,e^{-(L\,K_{\text{d}})}$ is the down-welling spectral irradiance of the background at wavelength λ, with $E_{\text{sun}}(\lambda, 0)$ at the sea surface [15]. Furthermore, T_w is the water transmittance, T_f and B_o are the transmittance and the bandwidth of the optical filter at the Rx. Then, I_i is passed through a trans-impedance amplifier (TIA) with load resistance R_{L}, followed by a low-pass filter (LPF) to limit the thermal noise n_{th}. The voltage signal at the LPF output is denoted by r_i:

$$r_i = R_{\text{L}}\,I_i + n_{\text{th}} = R_{\text{L}}\,\breve{I}_i + R_{\text{L}}\,n_{s_i} + n_{\text{th}}. \tag{5}$$

The total noise variance $\sigma^2_{n_i}$ is given by:

$$\begin{aligned}\sigma^2_{n_i} &= R^2_{\text{L}}\,(\sigma^2_{\text{sh},i} + \sigma^2_{\text{d}} + \sigma^2_{\text{b}}) + \sigma^2_{\text{th}} \\ &= R^2_{\text{L}}\,2\,e\,G\,F\,B_e\,(I_{s,i} + I_{\text{d}} + I_{\text{b}}) + 4\,K_{\text{Z}}\,T\,B_e\,R_{\text{L}}.\end{aligned} \tag{6}$$

where $\sigma^2_{\text{sh},i}$, σ^2_{d}, σ^2_{b}, and σ^2_{th} denote the variances of the signal shot noise, dark noise, background noise, and thermal noise, respectively. Here, e, G, K_{Z}, T, F, and B_e denote the electron charge, the SiPM gain, the Boltzmann constant, the Rx equivalent temperature in Kelvin, the PD excess noise factor, and the bandwidth of the Rx LPF, respectively.

Now, the electrical signal-to-noise ratio γ can be expressed as:

$$\begin{aligned}\gamma &= \frac{(R_{\text{L}}\,I_{s,1})^2}{\sigma^2_{n_1}} = \frac{(R_{\text{L}}\,\mathcal{R}_{\text{e}}\,P_{\text{Tx},1}\,h)^2}{R^2_{\text{L}}\,(2\,e\,G\,F\,B_e\mathcal{R}_{\text{e}}\,P_{\text{Tx},1}\,h + \sigma^2_{\text{d}} + \sigma^2_{\text{b}}) + \sigma^2_{\text{th}}} \\ &= \frac{\overbrace{(R_{\text{L}}\,\mathcal{R}_{\text{e}}\,P_{\text{Tx},1})^2}^{\mu^2}\,h^2}{\underbrace{2\,e\,G\,F\,B_e\,R_{\text{L}}\,\mu}_{\alpha}\,h + \underbrace{R^2_{\text{L}}\,\sigma^2_{\text{d}} + R^2_{\text{L}}\,\sigma^2_{\text{b}} + \sigma^2_{\text{th}}}_{\beta}} = \frac{\mu^2\,h^2}{\alpha\,h + \beta}.\end{aligned} \tag{7}$$

III. Link Ergodic Capacity

In our considered IM/DD scheme, the instantaneous channel capacity in bits per second per Hertz (bps/Hz) can be approximated as [16], [17]:

$$\begin{aligned}\mathcal{C} &\approx \frac{1}{2}\log_2\left(1 + \frac{\exp(1)\,\gamma}{2\,\pi}\right) \\ &\approx \frac{1}{2}\log_2\left(1 + \frac{\exp(1)}{2\,\pi}\left(\frac{\mu^2\,h^2}{\alpha\,h + \beta}\right)\right).\end{aligned} \tag{8}$$

The ergodic capacity in bps/Hz is obtained by averaging (8) over the PDF of h, $f_h(h)$:

$$\mathcal{C}_{\text{erg}} \approx \frac{1}{2}\int_0^\infty \log_2\left(1 + \frac{\exp(1)}{2\,\pi}\left(\frac{\mu^2\,h^2}{\alpha\,h + \beta}\right)\right) f_h(h)dh. \tag{9}$$

To derive $f_h(h)$ in (9), recall the definition of $h = h_c\,h_{\phi_{\text{t}}}\,h_{\phi_{\text{r}}}\,h_a$ in (2). We consider the Tx is attached beneath a

sea surface platform such as a buoy, which swerves as wind blows across it from different directions. Hence, we model the random angular misalignment of the Tx irradiance angle $\phi_{\rm t}$ as subject to the sea surface slope with the distribution as [6]:

$$f_{\phi_{\rm t}}(\phi_{\rm t}) = \frac{\tan(\phi_{\rm t})\sec^2(\phi_{\rm t})}{\sigma^2_{\phi_{\rm t}}} \exp\left(\frac{-\tan^2(\phi_{\rm t})}{2\sigma^2_{\phi_{\rm t}}}\right), \quad (10)$$

where $\sigma^2_{\phi_{\rm t}} = 0.003 + 0.00512\,U \pm 0.004$, and U is the wind speed in m/s [18]. Note that this model is valid for $1\,\text{m/s} < U < 14\,\text{m/s}$.

The Rx, mounted for instance on an AUV, is affected by underwater currents and AUV instability. For the sake of modeling simplicity, we assume the angular deviations $\phi_{\rm r}$ to be Gaussian distributed, with zero mean and variance $\sigma^2_{\phi_{\rm r}}$. The distribution of the Rx incidence angle ϕ_r is then:

$$f_{\phi_{\rm r}}(\phi_{\rm r}) = \frac{1}{\sqrt{(2\,\pi\,\sigma^2_{\phi_{\rm r}})}} \exp\left(\frac{-\phi^2_{\rm r}}{2\sigma^2_{\phi_{\rm r}}}\right), \quad (11)$$

Defining $h' = h_c\,h_{\phi_{\rm t}}\,h_{\phi_{\rm r}}$, its PDF can be obtained as [3]:

$$f_{h'}(h') = \int f_{h'|h_{\phi_{\rm r}}}(h'|h_{\phi_{\rm r}})\; f_{h_{\phi_{\rm r}}}(h_{\phi_{\rm r}})\; dh_{\phi_{\rm r}}, \quad (12)$$

where

$$f_{h'|h_{\phi_{\rm r}}}(h'|h_{\phi_{\rm r}}) = \frac{1}{h_{\phi_{\rm r}}} f_{h_0}\left(\frac{h'}{h_{\phi_{\rm r}}}\right)$$
$$= \frac{C_1}{m\,h'\sqrt{\left(\sqrt[m]{\frac{h'}{h_c h_{\phi_{\rm r}}}}\right)^{-2} - 1}}\; f_{\phi_{\rm t}}\left(\cos^{-1}\left(\sqrt[m]{\frac{h'}{h_c h_{\phi_{\rm r}}}}\right)\right), \quad (13)$$

$$f_{h_{\phi_{\rm r}}}(h_{\phi_{\rm r}}) = \frac{C_2}{\sqrt{1 - {h_{\phi_{\rm r}}}^2}}\; f_{\phi_{\rm r}}\big(\cos^{-1}(h_{\phi_{\rm r}})\big). \quad (14)$$

Here $h_0 = h_c\,h_{\phi_{\rm t}}$, and C_1 and C_2 are the normalization coefficients. Now, substituting (13) and (14) in (12) and applying inverse trigonometric rules, $f'_h(h')$ can be expressed as:

$$f_{h'}(h') = \int \frac{C_1\,C_2}{\sqrt{2\,\pi\,m^2\,h'^2\,\sigma^4_{\phi_{\rm t}}\,\sigma^2_{\phi_{\rm r}}\,\left(1 - {h_{\phi_{\rm r}}}^2\right)\left(\sqrt[m]{\frac{h'}{h_c\,h_{\phi_{\rm r}}}}\right)^4}}$$
$$\times \exp\left(\frac{\left(\sqrt[m]{\frac{h'}{h_c\,h_{\phi_{\rm r}}}}\right)^2 - 1}{2\sigma^2_{\phi_{\rm t}}\left(\sqrt[m]{\frac{h'}{h_c\,h_{\phi_{\rm r}}}}\right)^2}\right) \exp\left(-\frac{\left(\cos^{-1}(h_{\phi_{\rm r}})\right)^2}{2\,\sigma^2_{\phi_{\rm r}}}\right)\; dh_{\phi_{\rm r}}. \quad (15)$$

Therefore, overall, for $h = h'\,h_a$, the PDF of h can be obtained as:

$$f_h(h) = \int_0^\infty f_{h'}(h')\,f_{h|h'}(h|h')\,dh', \quad (16)$$

with

$$f_{h|h'}(h|h') = \frac{1}{h'}\,f_{h_a}\left(\frac{h}{h'}\right). \quad (17)$$

TABLE I
Simulation Parameters

Parameter	Value
LED wavelength λ	470 nm
LED peak transmit power P_{Tx_1}	1 W
OOK extinction ratio α	0.4
Bit rate $R_{\rm b}$	1 Mbps
Water transmittance T_w	≈ 0.97
Optical filter transmittance T_f	1
Optical filter bandwidth B_o	20 nm
Rx lens refractive index n_{rf}	1.5
LPF bandwidth B_e	$\approx R_{\rm b}/2$
SiPM active area $A_{\rm PD}$	9 mm^2
SiPM, number of SPADs	10998
SiPM gain G	10^6
SiPM responsivity $\mathcal{R}_{\rm e}$	7.58×10^{17} A/W
SiPM dark current $I_{\rm d}$	1.10 μA
SiPM excess noise factor F	1.1
TIA load resistance $R_{\rm L}$	1 kΩ

The PDF of h_a, which accounts for the link interruption when the incident beam angle is outside the Rx FoV, can be expressed as [19]:

$$f_{h_a}(h_a) = \left(\int_0^{\phi_{\rm FoVr}} f_{\phi_{\rm r}}(\phi_{\rm r})\,d\phi_{\rm r}\right)\,\delta(h_a - 1)$$
$$+ \left(1 - \int_0^{\phi_{\rm FoVr}} f_{\phi_{\rm r}}(\phi_{\rm r})\,d\phi_{\rm r}\right)\,\delta(h_a). \quad (18)$$

Using (16) and (17), $f_h(h)$ can be expressed as:

$$f_h(h) = f_{h'}(h) \int_0^{\phi_{\rm FoVr}} f_{\phi_{\rm r}}(\phi_{\rm r})d\phi_{\rm r} + \left(1 - \int_0^{\phi_{\rm FoVr}} f_{\phi_{\rm r}}(\phi_{\rm r})d\phi_{\rm r}\right)\delta(h). \quad (19)$$

IV. Numerical Results

We consider a vertical UWOC system operating at a link range (depth) of $L = 100\,\text{m}$ in clear waters with $K_{\rm d} \approx 0.08\,\text{m}^{-1}$ [15]. The Rx uses the blue-sensitive SiPM of SensL B-series MicroSB 30020 [20]. We neglect the effect of oceanic turbulence due to negligible variations in the water salinity and temperature, and further assume negligible Tx/Rx displacements, as compared to L. The Tx/Rx/link parameters are summarized in Table I. Although a relatively long range of 100 m was considered, solar irradiance has a non-negligible effect on the link performance due to using a highly sensitive photo-detector [21]. To calculate $\mathcal{C}_{\rm erg}$ analytically, (19) is used in (9), which is solved through numerical integration [22]. To validate the obtained results, we also calculate $\mathcal{C}_{\rm erg}$ via a statistical approach (i.e., simulation-based), where the capacity in (8) is averaged over 10^8 channel realizations (by generating random $\phi_{\rm t}$ and $\phi_{\rm r}$).

First, lets investigate the impact of link misalignment and the Tx/Rx parameters on the channel capacity. Figure 3 shows plots of $\mathcal{C}_{\rm erg}$ as a function of U for two values of m, assuming a relatively moderate angular misalignment with $\sigma_{\phi_{\rm r}} = 5^\circ$ at

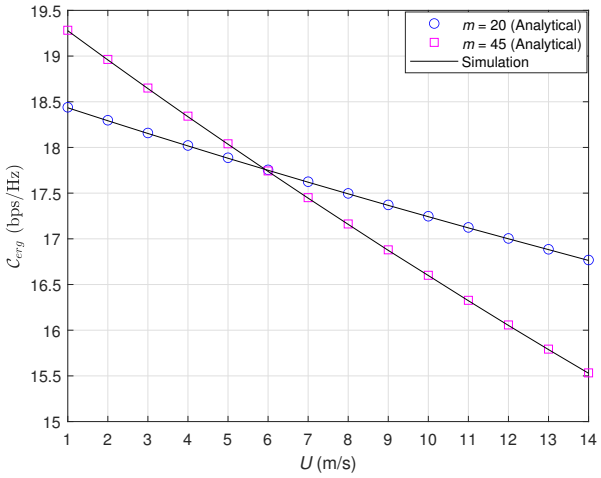

Fig. 3. Effect of surface wind speed U and Tx beam Lambertian order m on C_{erg}; $\sigma_{\phi_{\text{r}}} = 5°$, $\phi_{\text{FoVr}} = 20°$, $E_{\text{sun}}(0) = 1.8\,\text{Wm}^{-2}\text{nm}^{-1}$.

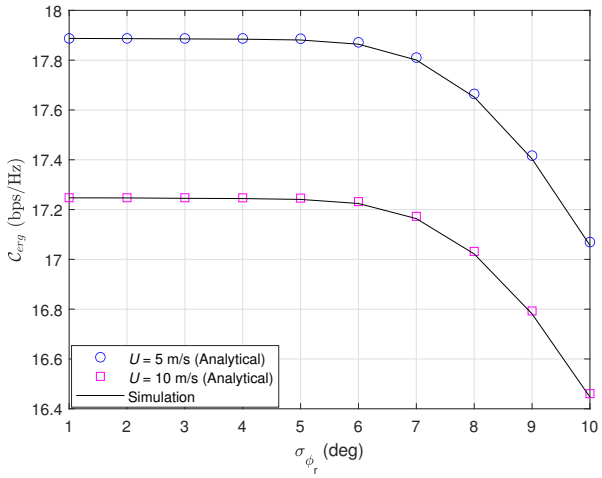

Fig. 4. Effect of Rx angular misalignment standard deviation $\sigma_{\phi_{\text{r}}}$ on C_{erg}; $m = 20$, $\phi_{\text{FoVr}} = 20°$, $E_{\text{sun}}(0) = 1.8\,\text{Wm}^{-2}\text{nm}^{-1}$.

the Rx with a FoV of 20°. The solar radiation irradiance at the water surface $E_{\text{sun}}(\lambda, 0)$ is set to $1.8\,\text{Wm}^{-2}\text{nm}^{-1}$, which corresponds to $\lambda = 470\,\text{nm}$ for the case of clear weather with the sun located at the zenith [23]. Firstly, notice the perfect match between analytically (indicated by circles and squares) and statistically calculated capacity values. Reasonably, $\mathcal{C}_{\text{erg}}$ decreases for deteriorated beam alignment due to increase in wind speed U, and the resulting reduced captured signal intensity on the PD. Also, note that for relatively small U, i.e., $U = 1 - 5\,\text{m/s}$, incurring relatively small pointing errors, a more directed beam with $m = 45$ (corresponding to semi-angle at half power $\phi_{\text{t},1/2} = 10°$) results in a higher capacity, compared to a wider beam with $m = 20$ ($\phi_{\text{t},1/2} = 15°$), due to a lower geometric loss for the former. For more significant pointing errors, e.g., for $U > 7\,\text{m/s}$, a more divergent beam should be used to relax the increased effect of pointing errors.

To see the effect of Rx angular misalignment, we have presented in Fig. 4 plots of $\mathcal{C}_{\text{erg}}$ as a function of $\sigma_{\phi_{\text{r}}}$ for $U = 5$ and $10\,\text{m/s}$ while setting $m = 20$ and the Rx FoV to 20°. Obviously, the capacity decreases with increased beam misalignment, i.e., a larger U and/or a more important $\sigma_{\phi_{\text{r}}}$. It is interesting to observe the 'waterfall' in both cases of $U = 5$ and $10\,\text{m/s}$ for $\sigma_{\phi_{\text{r}}} \gtrsim 6°$, which indicates that the considered Rx FoV of 20° can tolerate link misalignemnt for smaller $\sigma_{\phi_{\text{r}}}$.

Increasing the Rx FoV could be considered as a solution to reduce the effect of pointing errors related to the Tx angular misalignment (as a result of sea surface wind). However, at the presence of background radiations, increased FoV will also result in an increased level of Rx noise. To see the trade-off on the choice of the Rx FoV, we have presented in Fig. 5 plots of $\mathcal{C}_{\text{erg}}$ as a function of ϕ_{FoVr} for two values of solar irradiance at sea surface $E_{\text{sun}}(\lambda, 0)$ of 0.18 and $1.8\,\text{Wm}^{-2}\text{nm}^{-1}$. A moderate U of $6\,\text{m/s}$ and $\sigma_{\phi_{\text{r}}} = 5°$ are considered with $m = 20$. We notice that for relatively small values of the

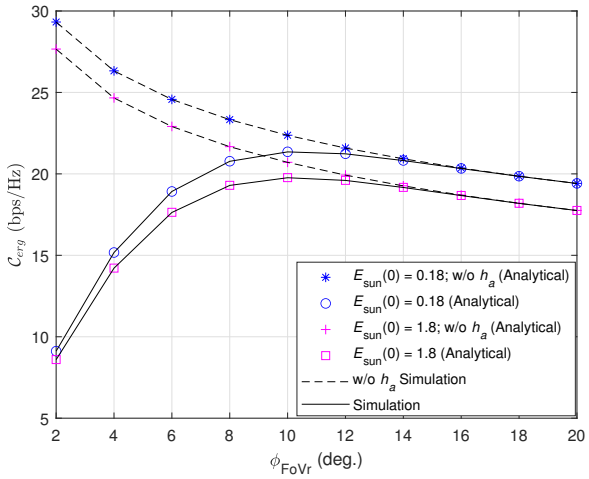

Fig. 5. Effect of the Rx Fov ϕ_{FoVr} and solar radiation irradiance at sea surface $E_{\text{sun}}(\lambda, 0)$ on C_{erg}; $m = 20$, $U = 6\,\text{m/s}$, $\sigma_{\phi_{\text{r}}} = 5°$.

Rx FoV (e.g., $\phi_{\text{FoVr}} < 6°$), the link is severely affected by the pointing errors, resulting in a relatively small capacity. On the other hand, for too large Rx FoV (e.g., $\phi_{\text{FoVr}} > 14°$), the link performance is affected by the increased captured background noise, which clearly shows the trade-off on the choice of ϕ_{FoVr}. As expected, a larger capacity is obtained for reduced background noise level, i.e., for a smaller $E_{\text{sun}}(\lambda, 0)$.

In order to better highlight the effect of beam misalignment for small FoV values, we have additionally shown $\mathcal{C}_{\text{erg}}$ plots (in dashed lines) by neglecting the link interruption (modeled by h_a in Equation (2)). We can clearly see that the decrease in $\mathcal{C}_{\text{erg}}$ for small FoV values is due to the link interruption. To further see the effect of link interruption, we have shown the histogram of the incidence angle at the Rx, ϕ_{r}, in Fig. 6 for $\sigma_{\phi_{\text{r}}} = 5°$. we can see that for $\phi_{\text{FoVr}} \gtrsim 14°$, ϕ_{r} mostly falls

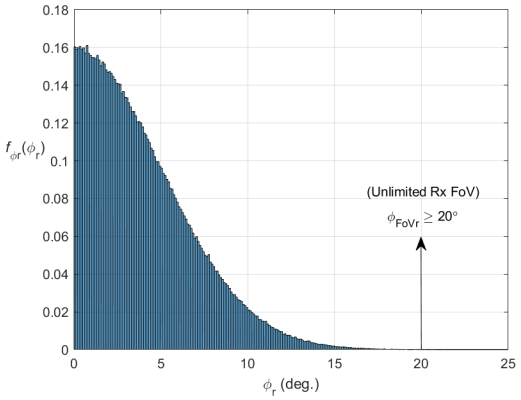

Fig. 6. Distribution of the angle of incidence ϕ_{r} for $\sigma_{\phi_{\mathrm{r}}} = 5^{\circ}$.

inside the Rx FoV, hence no link interruption occurs and the capacity is affected only by E_{sun}. Link interruption is dominant for $\phi_{\mathrm{FoVr}} \lesssim 8^{\circ}$, as can be also seen from Fig. 5.

V. Conclusions

We investigated the ergodic capacity performance of a downlink UWOC affected by Tx-Rx misalignment in the presence of background radiations. The presented distribution for the channel coefficient takes into account the effects of wind speed on the sea surface and the underwater unit instability. For a UWOC system design, the effects of link misalignment parameters and solar radiations, as well as Tx/Rx parameters, i.e., the Tx beam divergence, the Rx FoV, were studied on the channel capacity. The presented analytical results were further validated by statistical capacity calculations. In particular, we elucidated the trade-off in setting the Tx/Rx parameters based on link misalignment and solar radiation conditions.

References

[1] M. A. Khalighi, C. J. Gabriel, L. M. Pessoa, and B. Silva, *Visible Light Communications: Theory and Applications*. CRC-Press, 2017, ch. Underwater Visible Light Communications, Channel Modeling and System Design, pp. 337–372.

[2] H. Kaushal and G. Kaddoum, "Underwater optical wireless communication," *IEEE Access*, vol. 4, pp. 1518–1547, Apr. 2016.

[3] I. C. Ijeh, M. A. Khalighi, and S. Hranilovic, "Parameter optimization for an underwater optical wireless vertical link subject to link misalignments," *IEEE Journal of Oceanic Engineering*, vol. 46, no. 4, pp. 1424–1437, 2021.

[4] I. C. Ijeh, M. A. Khalighi, M. Elamassie, S. Hranilovic, and M. Uysal, "Outage probability analysis of a vertical underwater wireless optical link subject to oceanic turbulence and pointing errors," *IEEE/OSA Journal of Optical Communications and Networking*, in Press.

[5] Y. Dong, S. Tang, and X. Zhang, "Effect of random sea surface on downlink underwater wireless optical communications," *IEEE Communications Letters*, vol. 17, no. 11, pp. 2164–2167, Nov. 2013.

[6] H. Zhang, Y. Dong, and L. Hui, "On capacity of downlink underwater wireless optical mimo systems with random sea surface," *IEEE Communications Letters*, vol. 19, no. 12, pp. 2166–2169, Dec 2015.

[7] A. S. Ghazy, S. Hranilovic, and M.-A. Khalighi, "Angular MIMO for underwater wireless optical communications: Link modeling and tracking," *IEEE Journal of Oceanic Engineering*, vol. 46, no. 4, pp. 1391–1407, 2021.

[8] S. Arnon and D. Kedar, "Non-line-of-sight underwater optical wireless communication network," *J. Opt. Soc. Amer.*, vol. 26, no. 3, pp. 530–539, Mar. 2009.

[9] A. S. Ghazy, H. S. Khallaf, S. Hranilovic, and M. A. Khalighi, "Undersea ice diffusing optical communications," *IEEE Access*, vol. 9, pp. 159 652–159 671, 2021.

[10] M. A. Khalighi, T. Hamza, S. Bourennane, P. Léon, and J. Opderbecke, "Underwater wireless optical communications using silicon photo-multipliers," *IEEE Photonics Journal*, vol. 9, no. 4, 2017, dOI 10.1109/JPHOT.2017.2726565.

[11] A. Morel and L. Prieur, "Analysis of variations in ocean color," *Limnology and Oceanography*, vol. 22, no. 4, pp. 709–722, July 1977.

[12] J. M. Kahn and J. R. Barry, "Wireless infrared communications," *Proceedings of the IEEE*, vol. 85, no. 2, pp. 265–298, Feb 1997.

[13] *Introduction to SiPM, Technical Note*. ON Semiconductor® - SensL, 2011 (Rev. 6.0, Feb. 2017), available at https://www.sensl.com/downloads/ds/TN%20-%20Intro%20to%20SPM%20Tech.pdf.

[14] T. Hamza, M. A. Khalighi, S. Bourennane, P. Léon, and J. Opderbecke, "Investigation of solar noise impact on the performance of underwater wireless optical communication links," *Optics Express*, vol. 24, no. 22, pp. 25 832–25 845, Oct. 2016.

[15] C. Mobley, *Light and Water: Radiative Transfer in Natural Waters*. Academic Press, 1994.

[16] L. Yin and H. Haas, "Physical-layer security in multiuser visible light communication networks," *IEEE Journal on Selected Areas in Communications*, vol. 36, no. 1, pp. 162–174, 2018.

[17] M. Elamassie and M. Uysal, "Vertical underwater visible light communication links: Channel modeling and performance analysis," *IEEE Trans. Commun.*, vol. 19, no. 10, pp. 6948–6959, 2020.

[18] C. Cox and W. Munk, "Measurement of the roughness of the sea surface from photographs of the sun's glitter," *J. Opt. Soc. Amer.*, vol. 44, no. 11, pp. 838–850, Nov. 1954.

[19] M. T. Dabiri, S. M. S. Sadough, and M. A. Khalighi, "Channel modeling and parameter optimization for hovering UAV-based free-space optical links," *IEEE J. Sel. Areas Commun.*, vol. 36, no. 9, pp. 2104–2113, Sep. 2018.

[20] *B-Series Fast, Blue-Sensitive Silicon Photomultiplier Sensors datasheet*. SensL, 2013 (Rev. 3.1, Nov. 2015), available at http://www.sensl.com/downloads/ds/DS-MicroBseries.pdf.

[21] T. Hamza and M. Khalighi, "On limitations of using silicon photomultipliers for underwater wireless optical communications," *2nd West Asian Colloquium on Optical Wireless Communications (WACOWC)*, pp. 74–79, Apr. 2019, Tehran, Iran.

[22] *Numerical integration - MATLAB integral*. The MathWorks, Inc., 2020 (Ver. 9.8.0.1396136(R2020a)), available at https://www.mathworks.com/help/matlab/ref/integral.html.

[23] C. Mobley, E. Boss, and C. Roesler, *Ocean Optics Web Book*, http://www.oceanopticsbook.info/, last accessed: 16 Jan. 2022.